

RESEARCH PAPER

Low-Temperature Pulsed Laser Deposition for the Synthesis and Characterization of Nanopatterned Indium Tin Oxide on Glass Substrates for Gas Sensor Application

Naheda Humood*, Ahmed Shaker Hussein, Noora Al-janabi

Department of Basic Sciences, College of Dentistry, University of Babylon, Babylon, Iraq

ARTICLE INFO

Article History:

Received 12 June 2024

Accepted 20 September 2024

Published 01 October 2024

Keywords:

Gas Sensing

Indium Tin Oxide (ITO)

Low-Temperature Pulsed Laser Deposition (PLD)

Nanopatterned Thin Films

ABSTRACT

The results of this work exhibit the fabrication and characterization of nanopatterned ITO thin films on glass substrates through low temperature PLD for the purpose of gas sensing. The ITO films prepared at 25 °C displayed high transparency and conductivity, for their use in optoelectronics. X-ray diffraction (XRD) characterization disclosed a cubic form of In_2O_3 with particle size of about 33.64 nm while SnO_2 existed in a tetragonal form of about 14.57 nm. A mixed-phase sample of $\text{In}_2\text{O}_3:\text{SnO}_2$ exhibits well-defined peaks of both elements, proved the co-deposition process. The morphology of the nanoparticles was confirmed using FE-SEM, which revealed that the nanoparticles were spheroidal with a little aggregation and with an average size of 35-38 nm. Gas sensing evaluations revealed maximum sensitivity at a working temperature of 225°C, revealed by the changes in the resistance of ITO films exposed to 20 ppm ethanol vapor improving the carrier mobility of electrons. This optimized configuration and the low response time show that ITO thin films could potentially be used as ethanol gas sensors.

How to cite this article

Humood N., Hussein A., Al-janabi N. Low-Temperature Pulsed Laser Deposition for the Synthesis and Characterization of Nanopatterned Indium Tin Oxide on Glass Substrates for Gas Sensor Application J Nanostruct, 2024; 14(4):1169-1182. DOI: 10.22052/JNS.2024.04.017

INTRODUCTION

Indium tin oxide (ITO) plays a vital function in the practical uses of transparent conductive coatings across a broad spectrum of applications including electronic display devices, heat-reflective glass particularly for architectural and automotive industries and antireflective layers in numerous devices [1]. ITO has been remarkable as a wide-bandgap semiconductor which demonstrates high transmittance of light within the visible and near-infrared regions of the electromagnetic spectrum, accompanied by its ability to demonstrate high conductivity coexisting with high transmittance [2]. Such combination makes ITO a preferred material

for TCO, mostly for optoelectronic application such as OPVs and OLEDs. Furthermore, it also applies to increasing the efficiency of automobile as well as aircraft windows [3, 4]. Amid all TCOs, ITO reveals not only its optical and electrical characteristics but also a surface morphology, work function, as well as mechanical density and stability to various environments [5]. Both the structure and the function of the ITO films depend on the deposition method used for their formation. Some of the usual techniques are d.c magnetron sputtering, plasma assisted electron beam evaporation, sol-gel processing etc while others include CVD, oxygen ion-beam assisted deposition and PLD [6].

* Corresponding Author Email: dent.nahidh.hammoood@uobabylon.edu.iq



This work is licensed under the Creative Commons Attribution 4.0 International License.

To view a copy of this license, visit <http://creativecommons.org/licenses/by/4.0/>.

Of all the methods, the PLD method is especially peculiar for the fact that the chemical composition of the target material is preserved in the deposited film while the possibility to deposit at low substrate temperatures is suitable for the use of the plastic substrate [7]. Factors like oxygen gas pressure (PO₂) and the temperature of the substrate are vital factors which are critical in penetration in the process of PLD and determining the quality of the films acquiring [8]. For instance, reduction of PO₂ will increase the oxygen deficiencies and hence improve conductivity and carrier concentration. Similarly, raising the substrate temperature encourages larger grain sizes, effectively reducing grain boundary scattering and further boosting

conductivity [9, 10].

In this study, we will look at the synthesis of ITO nanoparticles with an average particle diameter less than 20 nm using PLD technique. We also examine the process of ITO films deposition to nanopatterned glass substrate without reheating of the substrate and at lower laser energy density. Furthermore, the films of ITO were coated on flat glasses to study the effect of texturing on the films. By examining the structural, elemental, morphological, optical, and electrical properties of the patterned films, there are additional discoveries which can be possibly useful in enhancing the possibility of patterned TCO films in the future. This work may well extend the capabilities and



Fig. 1. Illustrate the parts of the PLD system

Table 1. Illustrating characteristics of the laser system used

subject	Characterization
Laser model	Q-switched Nd: YAG nanosecond laser.
Laser wavelength	Fundamental (1064 nm) and second (532 nm), (1064 nm) in use.
Repetition rate	(1- 6) Hz, 6Hz in use.
Pulse duration	10 ns.
Laser energy	(200-800) mJ in use.
Spot size	2.2 mm

performance of organic optoelectronic devices and thereby contribute to the on-going process of developing this fast-growing technology.

MATERIALS AND METHODS

The nanostructure of a group of elements and oxides was prepared on a glass slide - after cleaning it with pure alcohol and using Nd: YAG laser device - (PLD) method, where high-purity metal sheets (99.99%) were used for the elements (In,Sn), with a diameter (1 cm) thickness (0.2 cm).

Equipment and device

An Nd: YAG laser with a pulsed Q-switch (Model HF -301, Huafei technology, China), with a focal length of 100 mm, a convex lens focused the laser beam, the laser gun, vacuum chamber.

Fig. 1 depict practically used laser system capable of preparing nanomembranes, with the specifications given in the Table 1. The concentrated Nd: As for the YAG Q-switching laser beam, the incidence of which through a window, makes an angle of 45° with the target surface. The relationships between the target and the substrate are arranged in such a way they are far enough from each other to ensure that the substrate holder does not interfere with the laser source. Some investigators modify the deposition process occasionally to achieve better deposition films using this process. To fabricate indium-tin oxide (ITO) nanostructures on a glass slide using the pulsed laser deposition (PLD) technique, the following is the procedure: This includes washing them adequately with pure alcohol, immersing them in alcohol and later washing them in deionized water. After that, the cleaned slide is put into an ultrasonic cleaning bath contain pure alcohol and sonicated for about 10 to 15 minute to ensure that it is free from contaminants. Afterward the slides are washed in deionized water and then dried on a slide drier or with the help of a lint-free cloth.

Following the preparation of the glass slides, we proceed to mount high-purity metal sheets of indium (In) and tin (Sn), each with a purity of 99.99%, diameter of 1 cm, and thickness of 0.2 cm, onto a suitable target holder within a vacuum chamber. It is essential to secure these targets to prevent any movement during the deposition process.

The next step involves setting up the PLD system, where we align the Nd: YAG laser system,

specifically the pulsed Q-switch model HF-301 from Huafei Technology, at a 45-degree angle to the target surface. A convex lens with a focal length of 100 mm is positioned to focus the laser beam onto the target material. We also adjust the spacing between the target and the substrate holder, ensuring there is sufficient distance for the laser beam to reach the target without obstruction. Before starting the deposition, we must create and maintain vacuum conditions in the chamber.

Deposition of ITO thin films through PLD starts with the pumping down of the chamber with a vacuum pump which brings the pressure range to 10^{-6} to 10^{-5} Torr to avoid the impact of atmospheric particles on the thin film deposition. Once optimal vacuum conditions are established, an Nd:YAG laser system is set by proper parameters; pulse energy of 300-500mJ and the frequency of 5-10 Hz as set in previous optimizing experiments. A laser beam is directed towards the targeted area and causes the ablation process to begin. As the pulsed laser engages the target material, the delivered energy initiates the rapid removal of the material surface through vaporization this produces a plasma plume composed of abated particles. These vaporized species then undergo condensation and solidification on the glass substrate in its final form of an ITO nanostructure. The deposition duration is also flexible and can take about thirty minutes to several hours depending on the required ITO layer thickness. After deposition is done it takes a period of time for the chamber to be restored to normal atmospheric pressure. The substrate, which has the deposited layer of indium tin oxide is then gently taken out of the substrate holder for evaluation on the coating uniformity of the surface of the glass also as well as the smoothness of the ITO layer deposited on the glass surface. optional, a post deposition heat treatment can be done to improve the crystallinity and electrical conductivity of the ITO layer, the treatment can be carried out in furnace in nitrogen or in vacuum at a temperature of 300-500 °C for 1-2 hours.

RESULTS AND DISCUSSIONS

X-ray diffraction also known as XRD is a well established method that used to study the crystal structure of sample. Two samples of indium oxide and Tin oxide thin films were deposited by employing two distinct physical PLD techniques. The XRD diffraction patterns of these samples

were different in terms of peak height and secondary peaks. For the X-ray diffraction patterns of the PLD grown In_2O_3 thin film deposited on glass substrates, refer to Fig. 2. The analysis of XRD diffractograms show that the In_2O_3 film formed at room temperature has a cubic structure [11]. Accuracy of (2θ) at (30.57) is attributed to plane (222) and at (35.45) , (45.69) , (51.02) , and (60.68) related to the plane (400) , (101) , (440) and (622) respectively. In Table 2 it can be noticed the structural parameters: The results are given in terms of 2θ , dhkl, FWHM and Crystallite size of

In_2O_3 . In general, increase of the crystalline size for In_2O_3 when FWHM decreased. On the basis of Scherrer's equation, the average crystalline size of the In_2O_3 NPs was found to be about 33.64 nm for the NPs synthesized via PLD.

The X-ray diffraction (XRD) analysis of the SnO_2 sample, as illustrated in Fig. 3, reveals distinct diffraction peaks corresponding to the crystallographic planes (110) , (101) , and (211) at 2θ diffraction angles of 26.7° , 33.97° , and 51.8° , respectively with Crystallite size (nm) 14.57 nm. These peaks signify the presence of a Tin crystal

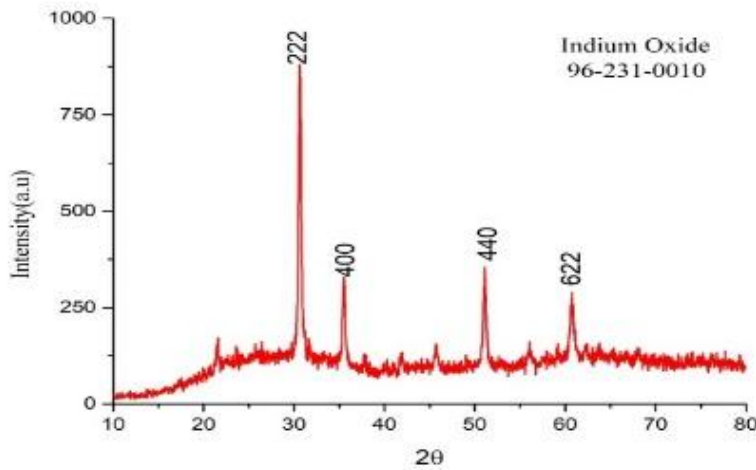


Fig. 2. XRD patterns of In_2O_3 NPs prepared by Physical PLD.

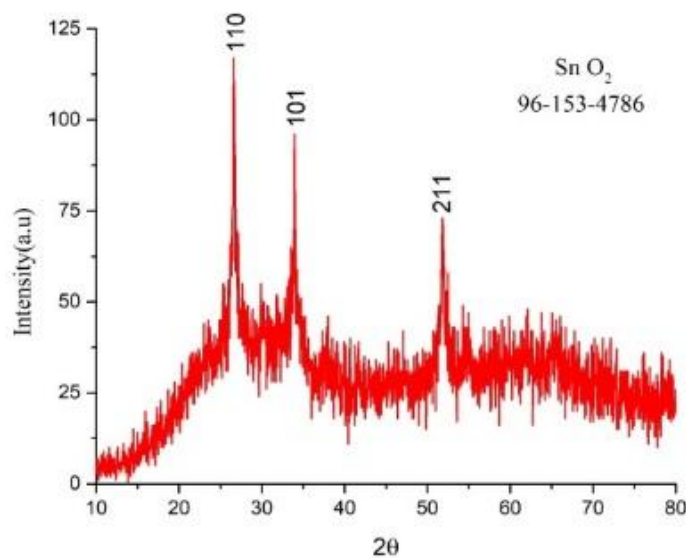


Fig. 3. XRD patterns of SnO_2 NPs prepared by PLD

Table 2. Structural parameters resulting from XRD of In_2O_3 and SnO_2 NPs

Samples	In_2O_3 NPs				SnO_2 NPs		
	Strongest peaks				Strongest peaks		
2 θ (Deg.)	30.65	35.52	51.1	60.76	26.7	33.97	51.8
FWHM (Deg.)	0.38	0.38	0.42	0.73	0.56	0.6	0.58
Crystallite size (nm)	21.6	22.05	20.79	12.61	14.57	13.65	15.72
Average Crystallite size (nm)	19.262				14.646		

Table 3. Structural parameters resulting from XRD of $\text{In}_2\text{O}_3:\text{SnO}_2$

2 θ (Deg.)	FWHM (Deg.)	dhkl STd.(Å)	dhkl Exp.(Å)	crystallite size (nm)	Average (nm)
25.45	0.32	3.57	3.50	25.45	
30.65	1.92	2.9761	2.91	4.29	
35.52	0.32	2.5294	2.53	26.07	17.13
51.11	0.48	1.7843	1.79	18.35	
60.73	0.80	1.5222	1.52	11.51	

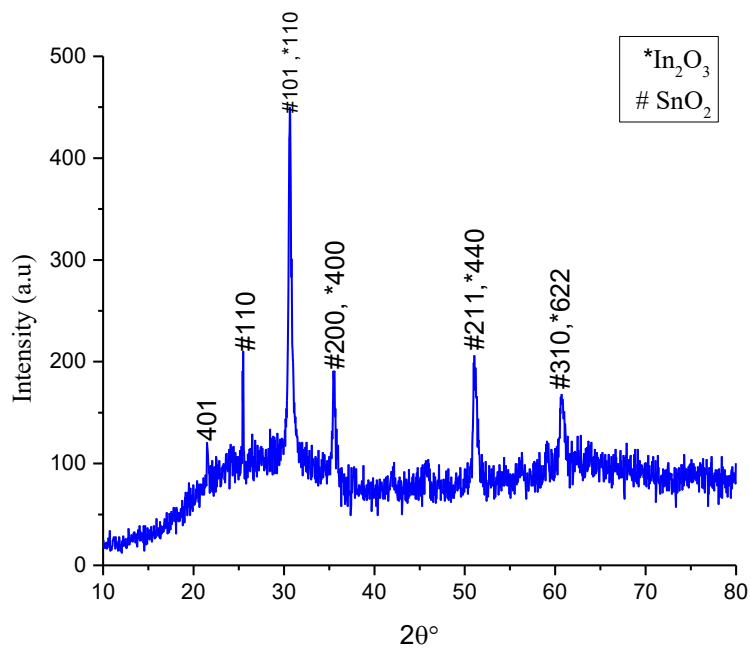


Fig. 4. XRD patterns of $\text{In}_2\text{O}_3:\text{SnO}_2$ prepared by PLD

phase characterized by a tetragonal structure, specifically designated by the Joint Committee on Powder Diffraction Standards (JCPDS) No. 96-153-4786 [12]. Upon closer examination, confirming the accuracy of the synthesis process.

The Fig. 4 show of X-ray diffraction (XRD) pattern of mixed phase composite sample of In_2O_3

Indium Oxide and SnO_2 Tin Oxide. It is possible to note the presence of several characteristic peaks in the diffraction pattern and their position shows certain crystallographic data of the sample. Thus, the highest peak of about 450 a.u. is associated with the most intensive reflex, which is typical for 30° (2θ) coinciding with the (101) crystal plane.

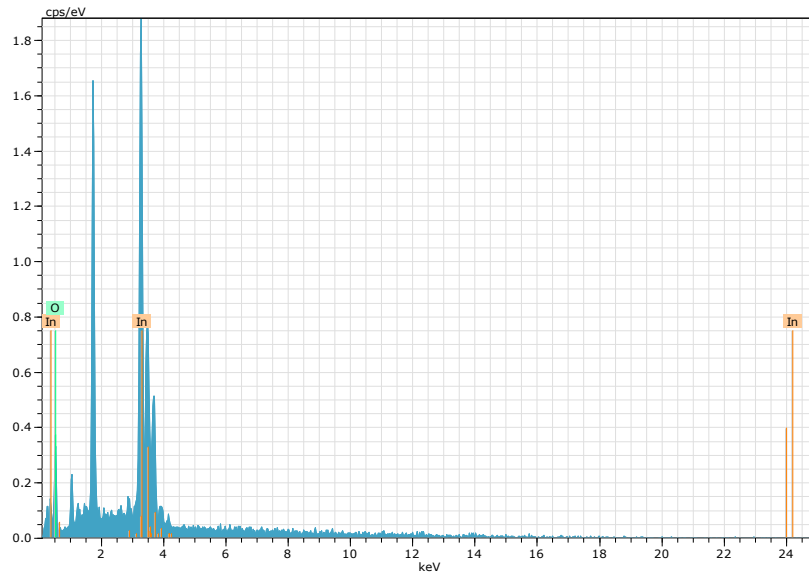


Fig. 5. EDX results of pure In_2O_3 NPs prepared by PLA and calcinated at 500 °C for 2 hours

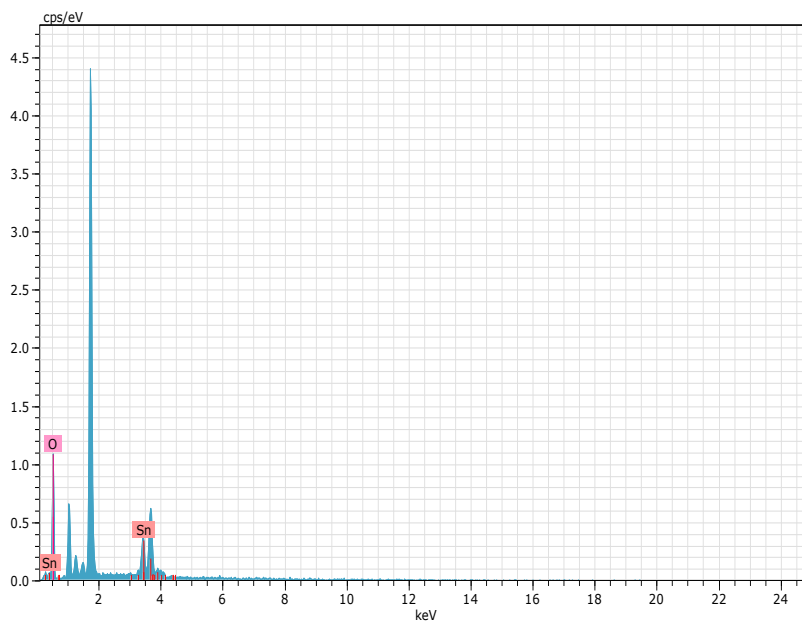


Fig. 6. EDX results of pure SnO_2 NPs prepared by PLA and calcinated at 500 °C for 2 hours

This sharp and high point together with other noticeable diffraction at different 2θ angles such as at $\sim 30^\circ$, $\sim 35^\circ$, $\sim 50^\circ$, and $\sim 60^\circ$ clearly demonstrates that this is a crystalline material with a definite crystal lattice structure. The indicated with (*) peaks are referred to the In_2O_3 phase, while the peaks indicated with (#) correspond to the SnO_2 phase, which proves the presence of both materials in the sample. However, the relatively sharp and

well-defined peaks indicate that the material is well crystalline. The background measurement noise seems quite low, which gives an impression of a very good quality measurement. The pattern ranges from 10° to 80° (2θ), which is usual for identifying basic crystallographic planes in oxide compounds. The observation of two major peaks from both phases alone makes one think that this could be an ITO (Indium Tin Oxide) [13].

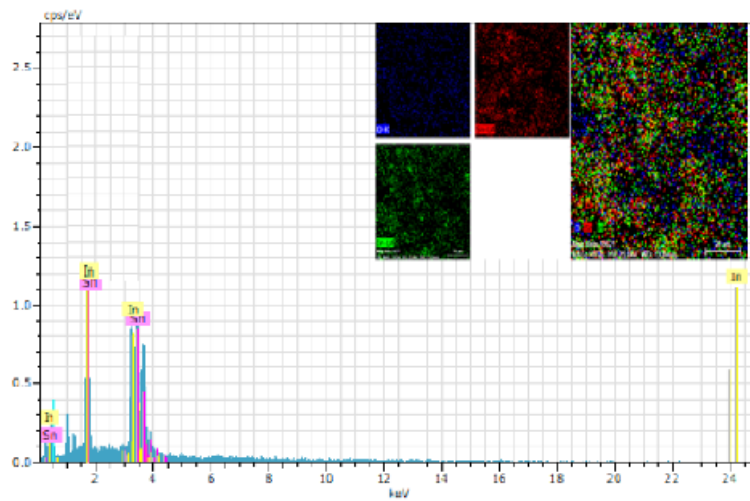


Fig. 7. EDX results of $\text{In}_2\text{O}_3:\text{SnO}_2$ NPs prepared by PLA and calcinated at 500°C for 2 hours

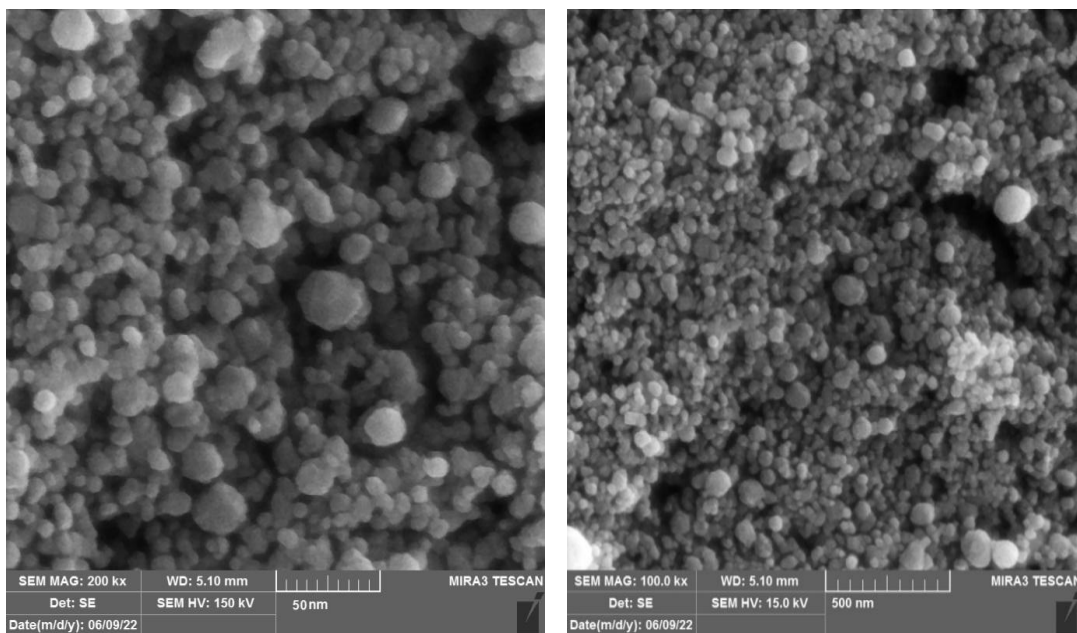


Fig. 8. FE-SEM image of In_2O_3 NPs prepared by PLA.

The EDS or EDX is an analytical method used to characterize a sample's chemical makeup or determine its elemental composition. The EDX technique was used in the current investigation to evaluate the NP's contents as well as any pollution that had been built up inside of them. Images from the EDX quantitative analysis of the samples are displayed in Fig. 4 and Fig. 5. The purity of the In_2O_3 and SnO_2 are calculated at 500°C for 2 hours respectively nanoparticles are confirmed by two significant peaks in each spectrum that correspond to In, Sn, and O. was discovered that the typical atomic percentages of In, and O.

In Fig. 7, we notice the appearance of an indium peak as well as the peaks of tin and the peaks of oxygen, which are between the last two peaks of indium and tin, the typical atomic percentages of In, Sn and O were between (29.54) ,(21.00)and (49.46), respectively.

Fig. 8 shows the FE-SEM image of In_2O_3 NPs prepared by PLD with average size about 35 nm and have spherical particles shape the shape of the spheroidal growth is clearly distinguished and the growth distribution is spread across the sample in a consistent manner

Fig. 8 shows the FE-SEM image of SnO_2 NPs

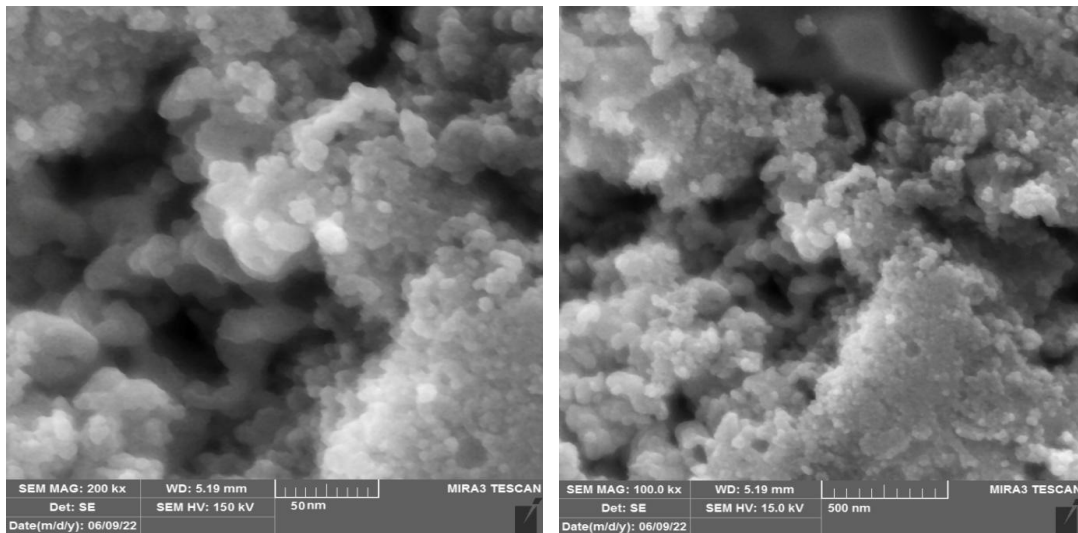


Fig. 9. FE-SEM image of SnO_2 NPs prepared by PLA

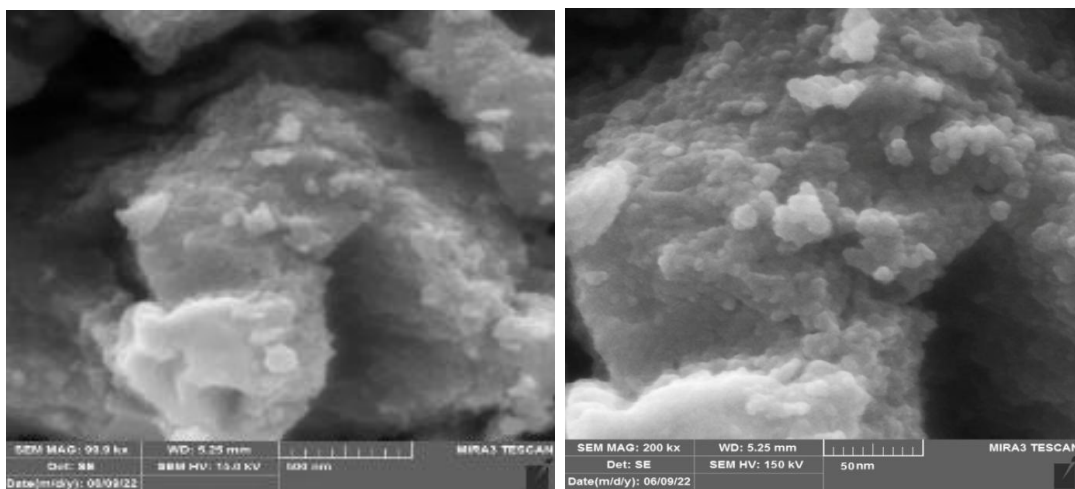


Fig. 10. FE-SEM image of $\text{In}_2\text{O}_3:\text{SnO}_2$ NPs prepared by PLA

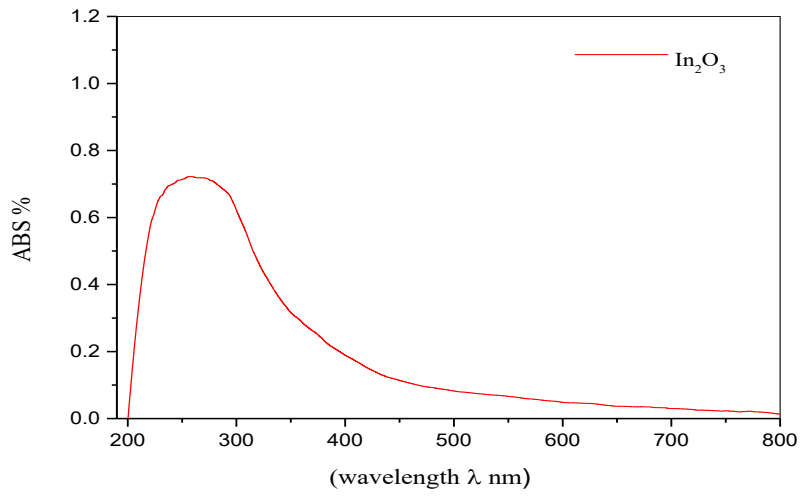


Fig. 11. UV-Visible absorbance of In_2O_3 NPs prepared by PLD

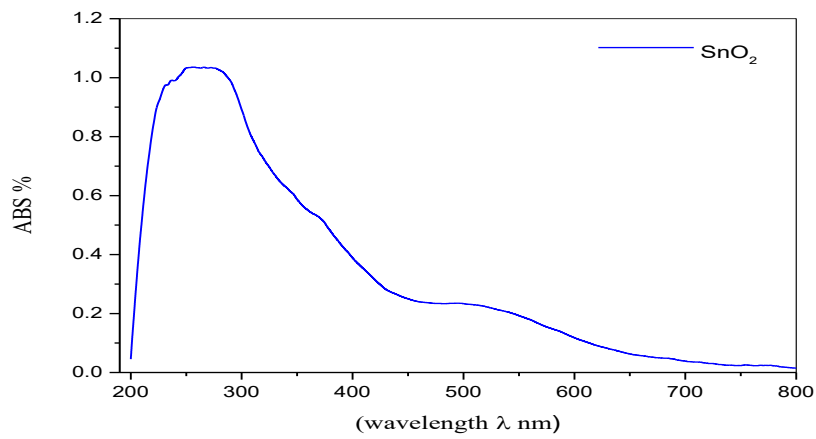


Fig. 12. UV-Visible absorbance of SnO_2 NPs prepared by PLD

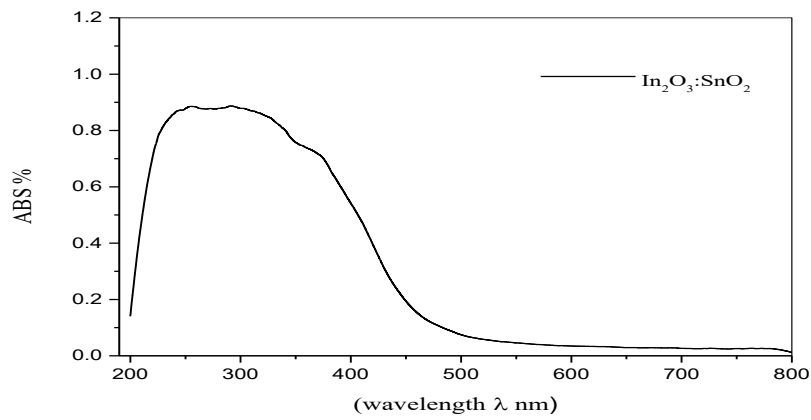


Fig. 13. UV-Visible absorbance of $\text{In}_2\text{O}_3:\text{SnO}_2$ NPs prepared by PLD

prepared by PLD with average size about 35 nm and have spheroidal particles shape but with a growth process accompanied by agglomeration of SnO_2 particles, which appears in Fig. 8 as bright regions. Assembly disease due to the finite size of nanoparticles with a growth rate distributed on all sides of the sample.

Fig. 10. shows the FE-SEM image of $\text{In}_2\text{O}_3:\text{SnO}_2$ NPs prepared by PLA with average size about 38 nm have spheroidal particles shape the increase in the size of the nanoparticles came as a result

of the physicochemical interaction of the tin ion with indium oxide during the process of ablation and plasma formation, which led to the growth of indium oxide on the tin oxide nanoparticles. Which, in turn, formed in a relatively larger size compared with the size of the individual elementary particles of both oxides

In Fig. 11, the absorbance spectrum of indium oxide, covers a broad range from 240 nm to 450 nm. This means that indium oxide nanoparticles are capable of absorbing light across this wavelength

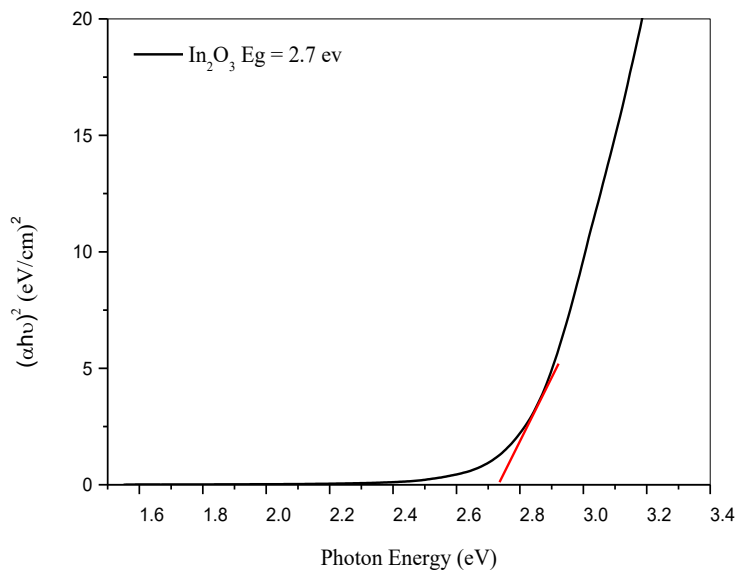


Fig. 14. Optical energy gap of the In_2O_3 prepared by PLD

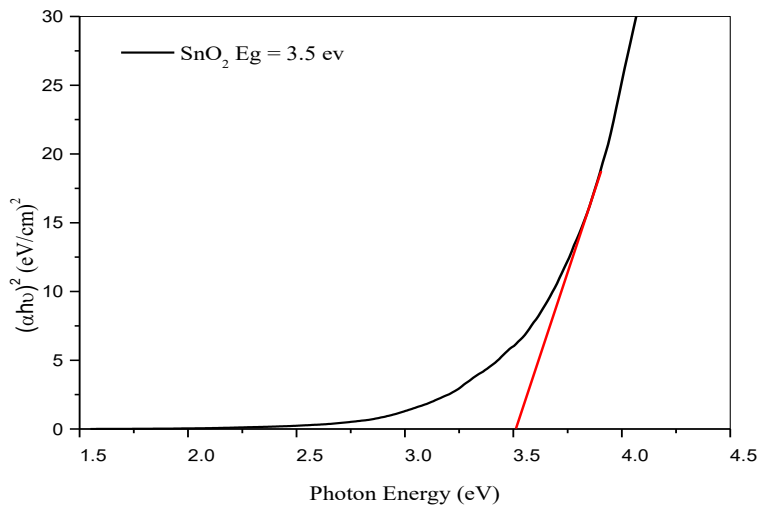


Fig. 15. Optical energy gap of the SnO_2 prepared by PLD

range. The breadth of this absorption spectrum indicates that indium oxide nanoparticles can interact with a wide range of light energies, making them versatile for various applications [14].

Fig. 12. Indicates the absorption spectrum of

SnO_2 , which falls within the low-wavelength range characterized by high-energy blue colors, extend from 200 nm to 350 nm. indicating its ability to absorb high-energy blue colors [15].

Fig. 13 demonstrates the optimal absorption

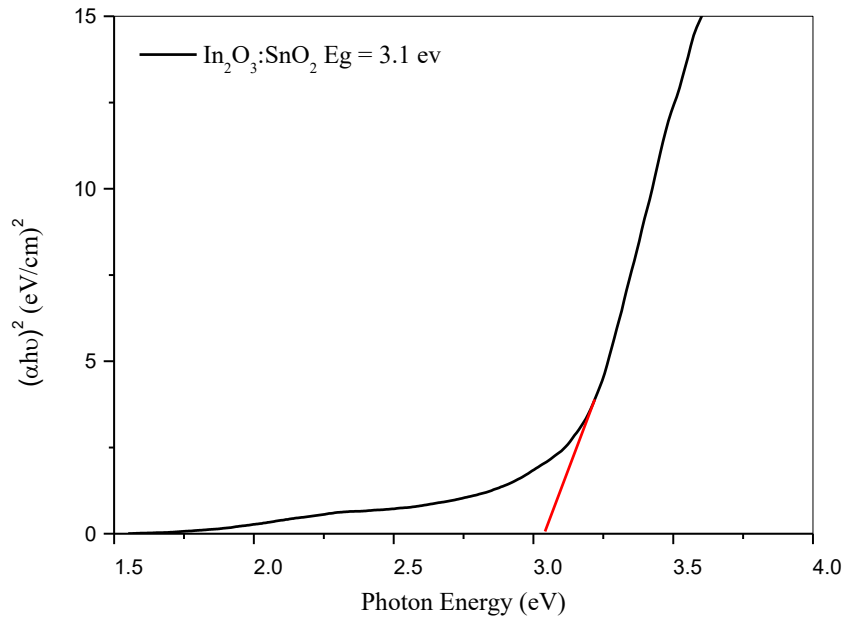


Fig. 16. Optical energy gap of the $\text{In}_2\text{O}_3:\text{SnO}_2$ prepared by PLD

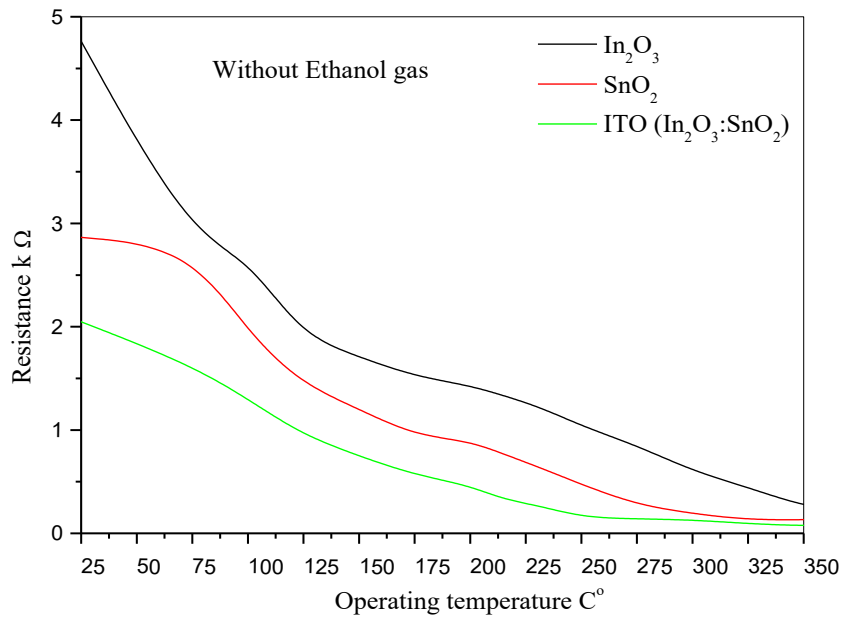


Fig. 17. Resistance of In_2O_3 , SnO_2 , and $(\text{In}_2\text{O}_3:\text{SnO}_2)$ vs. operating temperature without Ethanol gas

characteristics observed in prepared through the Biochemical method. Specifically, when indium oxide is prepared with tin oxide, in Fig. 13, the absorption range significantly widens while maintaining consistent intensity levels, which are indicative of the density of the prepared nanoparticles. The absorption capacity extends broadly from 200 nm to 500 nm due to the overlap

of sub-energy levels.

Figs. 14, 15 and 16 show the energy gap was measured for three samples (In_2O_3 , SnO_2 , and $\text{In}_2\text{O}_3\text{-SnO}_2$) which were prepared by the PLD method. the E_g was 2.7eV, 3.5ev, and 3.1 respectively.

Fig. 17 makes it evident that all films' resistance decreases as operating temperature rises before

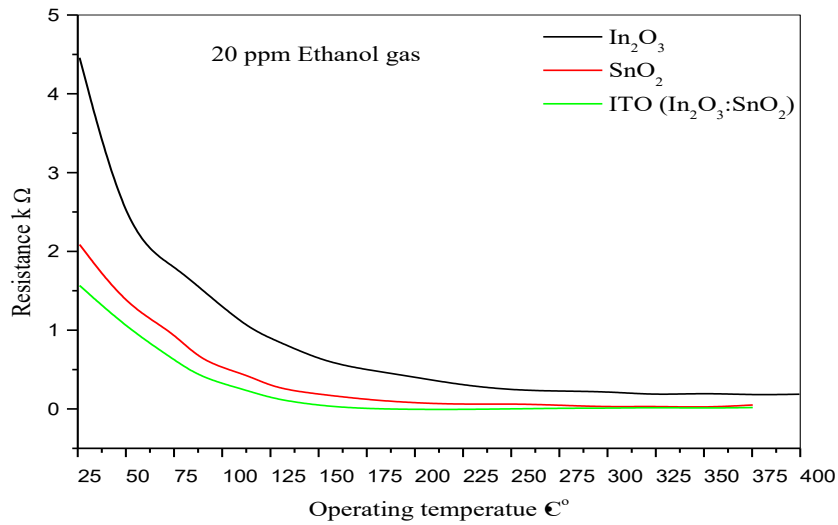


Fig. 18. Resistance of In_2O_3 , SnO_2 , and ($\text{In}_2\text{O}_3:\text{SnO}_2$) vs. operating temperature with Ethanol gas

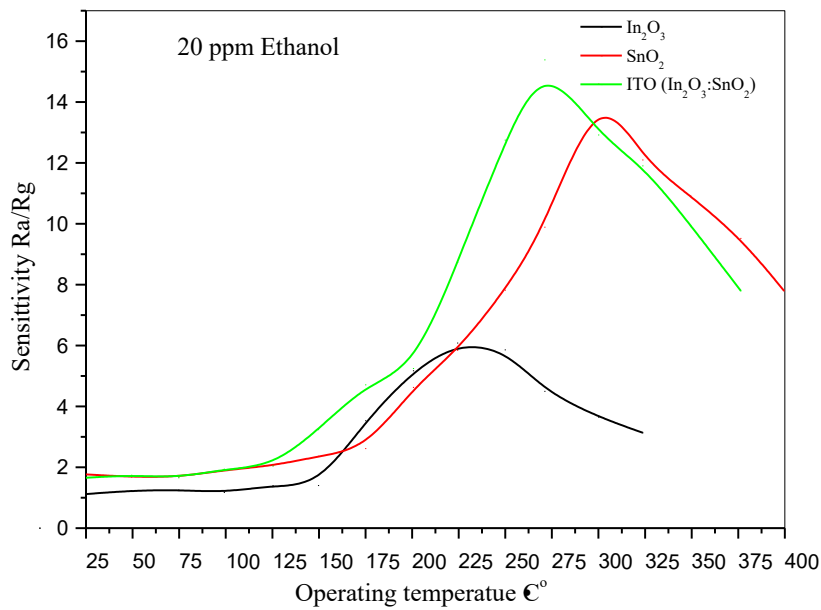


Fig. 19. Sensitivity of In_2O_3 , SnO_2 , and ($\text{In}_2\text{O}_3:\text{SnO}_2$) vs. operating temperature exposed to 20ppm Ethanol gas

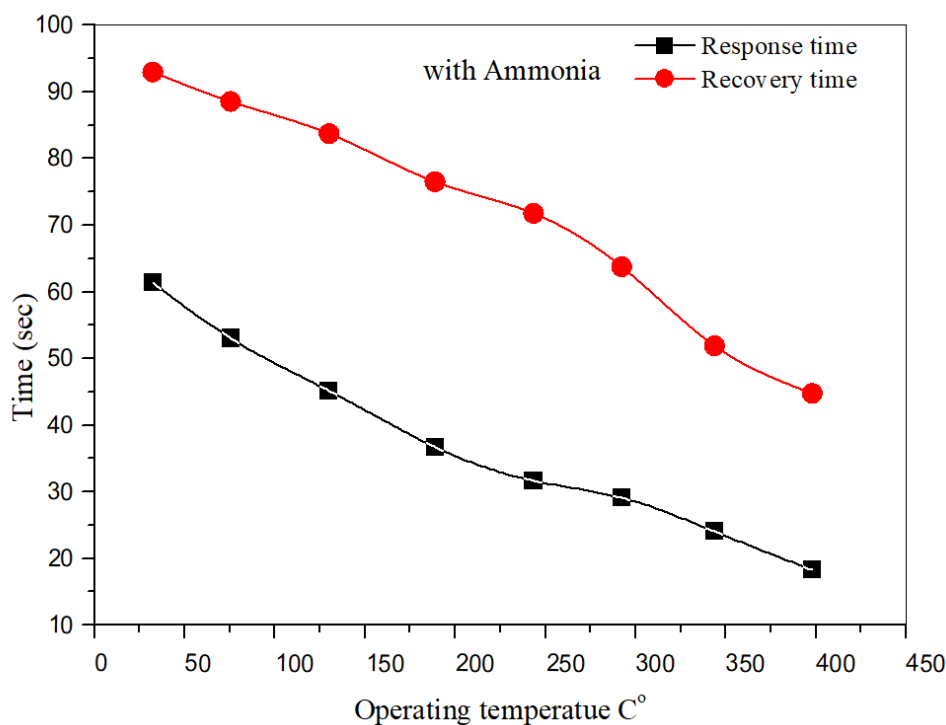
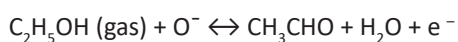


Fig. 20. Response time and recover time of ($\text{In}_2\text{O}_3:\text{SnO}_2$) vs. operating temperature exposed to 20ppm Ethanol

exposure to ethanol vapor; this is because all films are semiconductors, and it has been noted in a number of metal oxides. The behaviour of R_a Ω whole can be divided into three distinct temperature ranges: (i) low temperature, where oxygen is physisorbed on the surface of films and absorbs electrons from their interiors; (ii) moderate temperature, where physisorbed oxygen species (O) are converted into chemisorbed oxygen (O^-), resulting in a decrease in R_a ; and (iii) higher temperature, where R_a shows a decrease with increase in temperature due to the semiconductor behavior, it is evident that the resistance decreases;

Fig. 17 shows the variation of sensor resistance prepared at different materials substrate of ($\text{In}_2\text{O}_3:\text{SnO}_2$) after exposure to the 20-ppm ethanol gas.



The process releases electrons, increasing carrier concentration and thinning the depletion layer in the sensors In_2O_3 , SnO_2 , and $\text{In}_2\text{O}_3:\text{SnO}_2$ NPs. This results in decreased electrical resistance

and increased conductivity, especially in $\text{In}_2\text{O}_3:\text{SnO}_2$ NPs, where the high surface-to-volume ratio enhances gas reactions and further reduces resistance.

Fig. 18 illustrates how the sensitivity of three sensor In_2O_3 , SnO_2 , and $\text{In}_2\text{O}_3:\text{SnO}_2$ respectively varies with operating temperature in the range (25-400°C). It has been discovered that the sensitivity of In_2O_3 , SnO_2 , and ($\text{In}_2\text{O}_3:\text{SnO}_2$) films increases with rising operating temperature, peaks at the ideal temperature(200Co), then declines The activation energy to finish the chemical reaction at 350Co temperature. The optimum working temperature was determined at 250 °C for In_2O_3 , $\text{In}_2\text{O}_3:\text{SnO}_2$, sensors. The $\text{In}_2\text{O}_3:\text{SnO}_2$ films, which exhibits a maximum response at 225°C which is attributed to a decrease of defect of NPs which leads to increase in mobility carriers. A better improvement in the sensitivity and operating temperature is seen in our case than in the earlier reports

The response and the recovery times are important parameters for designing sensors for the desired applications. For an efficient gas sensor, the sensitivity should be high while

response and recovery time should be small. The response time is the time taken by a sensor to achieve 90% of the total resistance change in the case of the adsorption process, or the recovery time in the case of the desorption process. The response time and recovery time of $(\text{In}_2\text{O}_3:\text{SnO}_2)$ prepared and exposed to 20 ppm ethanol at an optimum working temperature of 225°C shown in Fig. 20. The results of response and recovery time at different substrate materials to determine the optimum working temperature and lowest response time and recovery time is shown that the response time and the recovery time decrease in, Fig. 19 shows that when the operating temperature increase of both response time and recovery time is decreased, the rise in temperature causes faster response and longer recovery times for the sensor.

CONCLUSION

Developing special nanopatterned structures on ITO thin films prepared by the low-temperature PLD method for glass substrates, the films exhibit excellent optical and gas-sensing properties. The films shown the appropriate crystallite size (33.64 nm In_2O_3 and 14.57 nm SnO_2) for high sensitivity. The structural coherency and preferably increased ethanol gas sensitivity at 225°C indicate possible use of ITO films in sensor fields. Moreover, the ITO samples possessed good stability and short response time, which could be considered as practical requirements for the gas-sensing devices. These results advance the understanding of the fact that low-temperature PLD is an efficient method for preparing high-quality ITO thin films for optoelectronic and sensing applications.

CONFLICT OF INTEREST

The authors declare that there is no conflict of interests regarding the publication of this manuscript.

REFERENCES

- Maniyara RA, Graham C, Paulillo B, Bi Y, Chen Y, Herranz G, et al. Highly transparent and conductive ITO substrates for near infrared applications. *APL Materials*. 2021;9(2).
- Yuvaraja S, Khandelwal V, Tang X, Li X. Wide bandgap semiconductor-based integrated circuits. *Chip*. 2023;2(4):100072.
- Jung HS, Han GS, Park N-G, Ko MJ. Flexible Perovskite Solar Cells. *Joule*. 2019;3(8):1850-1880.
- Sharme RK, Quijada M, Terrones M, Rana MM. Thin Conducting Films: Preparation Methods, Optical and Electrical Properties, and Emerging Trends, Challenges, and Opportunities. *Materials* (Basel, Switzerland). 2024;17(18):4559.
- Mondal I, Saha Y, Halder P, Mondal D, Kundu M, Bhattacharya D, et al. Synchronization of theoretical and experimental studies on the enriched optical and dielectric properties of size modulated CoCr_2O_4 quantum dots. *Solid State Sciences*. 2023;146:107342.
- Shakiba M, Kosarian A, Farshidi E. Effects of processing parameters on crystalline structure and optoelectronic behavior of DC sputtered ITO thin film. *Journal of Materials Science: Materials in Electronics*. 2016;28(1):787-797.
- Gondoni P, Ghidelli M, Di Fonzo F, Russo V, Bruno P, Marti-Rujas J, et al. Structural and functional properties of Al:ZnO thin films grown by Pulsed Laser Deposition at room temperature. *Thin Solid Films*. 2012;520(14):4707-4711.
- Ichino Y, Yoshida Y, Takai Y, Matsumoto K, Ikuta H, Mizutani U. Influences of oxygen pressure and substrate temperature on the quality of $\text{NdBa}_2\text{Cu}_3\text{O}_x$ thin films prepared by pulsed laser deposition. *Superconductor Science and Technology*. 2004;17(6):775-780.
- Zhou M, Li J, Dong G, Gao S, Feng J, Liu R. Enhancement of Thermoelectric Performance for InTe by Selective Substitution and Grain Size Modulation. *Crystals*. 2023;13(4):601.
- Sung Y, Malay RE, Wen X, Bezama CN, Soman VV, Huang M-H, et al. Anti-reflective coating with a conductive indium tin oxide layer on flexible glass substrates. *Appl Opt*. 2018;57(9):2202.
- Yaragani V, Kamatam H, Deva Arun Kumar K, Mele P, Christy A, Gunavathy K, et al. Structural, Magnetic and Gas Sensing Activity of Pure and Cr Doped In_2O_3 Thin Films Grown by Pulsed Laser Deposition. *Coatings*. 2021;11(5):588.
- Debataraja A, Zuhendri DW, Yuliarto B, Nugraha, Hiskia, Sunendar B. Investigation of Nanostructured SnO_2 Synthesized with Polyol Technique for CO Gas Sensor Applications. *Procedia Engineering*. 2017;170:60-64.
- Hakimi AMHR, Banerjee N, Aziz A, Robinson JWA, Blamire MG. Estimating the spin diffusion length of semiconducting Indium Tin Oxide using Co/Indium Tin Oxide/Co spin valve junctions. *Appl Phys Lett*. 2010;96(10).
- Jothibas M, Manoharan C, Johnson Jeyakumar S, Praveen P. Study on structural and optical behaviors of In_2O_3 nanocrystals as potential candidate for optoelectronic devices. *Journal of Materials Science: Materials in Electronics*. 2015;26(12):9600-9606.
- Chen C, Zhang W, Li Y, Cai C. Defect-related optical bandgap narrowing and visible photoluminescence of hydrothermal-derived SnO_2 nanoparticles. *Journal of Materials Science: Materials in Electronics*. 2017;28(24):18603-18609.